Solar Energy 242 (2022) 267–275

Contents lists available at ScienceDirect

Solar Energy

journal homepage: www.elsevier.com/locate/solener

Silicon solar cell production line and key performance indicators: A case of study at front size serigraphy stage

M.C. López-Escalante [a,*], J.J. Peinado-Pérez [b], S. Palanco [b], J.R. Ramos-Barrado [b], F. Martín [a]

[a] The Nanotech Unit, Laboratorio de Materiales y Superficies and Departamento de Ingeniería Química, Facultad de Ciencias, Universidad de Málaga, Málaga 29071, Spain

[b] The Nanotech Unit, Laboratorio de Materiales y Superficies and Departamento de Física Aplicada, Facultad de Ciencias, Universidad de Málaga, Málaga 29071, Spain

ARTICLE INFO

Keywords:
Silicon photovoltaic
Serigraphy
Silver reduction
Real production data

ABSTRACT

Photovoltaic industry has devices power improvement as a main target. This implies that technological advances are continuously implemented in production lines and their power improvements have to be monitored with the suitable key performance indicators. In this work, front size serigraphy design has been selected as process improvement and laminated unit power and cell to module ratio has been defined as the main key performance indicator. Real size silicon PV cells with three different front finger morphologies have been produced in industrial production lines by the use of two front size serigraphy designs. The modification of the finger dimensions (wide/height) from (183.0 μm/31.6 μm) to (184.0 μm/37.6 μm) and (140.0 μm/40.8 μm) leads to a redistribution of the majority produced cell power range from [4.10–4.15) W to [4.10–4.15) W and [4.20–4.25) W respectively. Concerning the cell production, it has successfully been monitored by the laminated unit power indicator along a month when shows an increment from 3.95 W to 4.20 W. Concerning module level, cell to module ratio per process cell range is selected as suitable indicator and monitoring during a year. In the specific case of [4.30–4.35) W cell range, cell to module ratio decrease from 7.7 % to 6.5 %

1. Introduction

The Paris Agreement (2015) was the first time that something momentous happened concerning climate change: every country agreed to work together to limit the global warming to well below 2 degrees, preferably to 1.5 degrees, and recognizing the need for financial funding to combat climate change (https://www.miteco.gob.es/es/cambio-climatico/temas/el-proceso-internacional-de-lucha-contra-el-cambio-climatico/naciones-unidas/elmentos-acuerdo-paris.aspx). The last Conference of the Parties, COP26, presents climate change as a global priority and asks countries to come forward with ambitious 2030 emission reduction targets that align with reaching net zero by the middle of the century (https://ec.europa.eu/clima/policies/strategies/2050_en; JRC Science for Policy Report, 2019; , Jäger-Waldau., 2022). To deliver on these ambitious targets, COP26 has defined four strategic working lines: accelerating the phase-out of coal, curtailing deforestation, speeding up the switch to electric vehicles and encouraging the investment in renewables (https://ukcop26.org/cop26-goals/).

These four topics aim to change the structure of global energy demand: a decreasing role of fossil fuels, offset by an increasing share of renewable energies and a growing role for electricity. Indeed, during 2020, renewable energy generation (including biofuels but excluding hydro) increased by 9.7 %, somewhat slower than in previous years due to the pandemic, although the increase in absolute energy terms (2.9 EJ) was similar to the increases observed in 2017, 2018 and 2019 (https://www.bp.com/content/dam/bp/business-sites/en/global/corporate/pdfs/energy-economics/energy-outlook/bp-energy-outlook-2020.pdf; https://www.bp.com/content/dam/bp/business-sites/en/global/corporate/pdfs/energy-economics/statistical-review/bp-stats-review-2021-full-report.pdf). In the specific case of photovoltaic solar energy (PV), the predicted global market demand will be above 150 GW_p in 2021 (https://itrpv.vdma.org/documents/27094228/29066965/2021%30ITRPV/08ccda3a-585e-6a58-6afa-6c20e436cf41), a value which will be readily reached since the global PV module production capacity will exceed 300 GW_p achieved in 2020 due to continued capacity expansions (https://itrpv.vdma.org/documents/27094228/29066965/2021%30ITRPV/08ccda3a-585e-6a58-6afa-6c20e436cf41). This over-capacity of production implies a price freeze and prevents the possibility of any increase in production costs in the entire value chain: from wafer to modules, through cells. The pressure on cost reductions in

* Corresponding author.
E-mail address: mclopez@uma.es (M.C. López-Escalante).

https://doi.org/10.1016/j.solener.2022.07.005
Received 15 March 2022; Received in revised form 26 June 2022; Accepted 7 July 2022
Available online 22 July 2022

consumables and materials will be higher and it will be transferred to existing manufacturing lines with the objective to achieve a higher productivity and to improve product performance (https://itrpv.vdma.org/documents/27094228/29066965/2021%30ITRPV/08ccda3a-585e-6a58-6afa-6c20e436cf41; United Nations, 2015; United Nations, 2015).

Concerning cost reductions in materials, the most expensive non-silicon materials used in current mono-crystalline silicon solar cells (mono-Si) are undoubtedly metallization pastes or inks. The average silver quantity included in a 166 × 166 mm mono-Si cell size was 90 mg in 2020 and about 80 mg in 2021 for standard PERC monofacial (https://itrpv.vdma.org/documents/27094228/29066965/2021%30ITRPV/08ccda3a-585e-6a58-6afa-6c20e436cf41). The silver price was 840 USD/kg at the beginning of March 2021, with a 50 % increase over one year 11 (Lowell, 2001). This implies a cost of 7.5 USD cents/cell or in other words, 1.2 USD cents/W_p for a 22.5 % efficiency mono PERC cell, nearly 60 % of the non-wafer mono cell price. For this reason, it is necessary to consider such silver reduction as a technology evolution where the aggressive target of a reduction to 50 mg per cell within the next 10 years for PV cells, cannot achieved by a single change in the PV cell process, but through a sequence of perfectly coordinated changes which will imply suitable frontal silver ink formulations, re-design of the frontal serigraphy meshes, and the monitorization of these advances directly on the production line (https://itrpv.vdma.org/documents/27094228/29066965/2021%30ITRPV/08ccda3a-585e-6a58-6afa-6c20e436cf41).

Although the silver paste is a close formulation of the supplier, the general lines of the serigraphy design are well known. They should allow the printing of taller and thinner fingers as well as increasing the number of busbars. This configuration seeks to reduce the shadowing while keeping the line contact resistance at a low value, a low rate of finger interruptions and an increase of the output power per cell. The final target to be achieved for the coming ten years is to achieve a finger width of 20 μm in combination with layouts of 5, 6 or even more busbars and double printing technology, which implies an intensive work with the production mesh alignment (https://itrpv.vdma.org/documents/27094228/29066965/2021%30ITRPV/08ccda3a-585e-6a58-6afa-6c20e436cf41; Current price and price trend of gold and silver; Glunz, 2007; Glunz, 2007). The changes that will be carried out at production lines during this decade will require an accurate quantification in order to plan the roadmap (Hörteis and Glunz, 2008; Caballero, 2010; Papetti et al., 2019; Salahi and Jafari, 2016; May et al., 2015; Kourkoumpas et al., 2018). Every change implemented in the production lines will follow the planed roadmap and the only way to determine the deviations with respect to the established objective is through monitorization. In a factory, this monitoring is done through key production indicators (KPI), which for the present case will quantify the power generated by each cell produced (Ferrer et al., 2018; Bhadani et al., 2020; Kourkoumpas et al., 2018; Navas-Anguita et al., 2020; Chauvy et al., 2019; Matino et al., 2017; Gallo et al., 2020; Hu et al., 2020; Li et al., 2020). Despite the relevance of these KPI they are not defined by a specific PV normative. This means that each solar cell producer will be the responsible of defining its own KPI to comprehend and evaluate any innovative tool implemented at its production lines.

In this work, we present a successful case study on a total frontal serigraphy change (design and paste) and its valorization into a real production line using KPI, a case study which is absolutely in-line with PV industry roadmap for the next ten years. Three different candidate designs were assessed in the cell line with a single printing technology. In addition, each of the designs (i.e., the old one and the candidates) were accompanied by a silver paste formulation developed by DuPont (a chemical analysis of the paste is out of the scope of this work). The efficiency variations introduced by the various designs and pastes were revealed by defining both a cell-level and a module-level KPI. The data presented is the result of the monitoring of both KPI during a whole year of production.

2. Material and methods

The experimental section has been structured in two parts. The first one is devoted to the morphological and electrical characterization of the two front size serigraphy designs of the printed finger. The second one is dedicated to the electrical characterization of the fabricated PV cells and modules for each serigraphy design and its respective KPI: Lam-UP for the cells and CMR for the modules.

With regards to the PV cell study, all the analyzed devices are p-type Cz-Si wafers with a surface area of 238.95 cm^2, 180–200 μm thick, base resistivity between 1.0–3.0 Ω × cm, and minority carrier lifetime higher than 12 μm. The solar cell fabrication process starts with the alkaline texture stage with the aim to generate the well-known pyramidal structure. After that, the phosphorous diffusion profile is developed. Then, the phosphorus glass is removed, and the silicon nitride antireflection coating is deposited. The following stage is dedicated to generating the front and back size metallic contacts and finally the laser isolation followed by the PV cell measurement and sorting is carried out. Regarding the front size serigraphy stage, two screen-printing designs (S1 and S2) and two silver paste formulations (P1 and P2) have been considered. Both screen-printing designs print 58 fingers but with different thickness: 125 μm and 90 μm for S1 and S2, respectively. The paste chemical formulation is out of the scope of this work, but it is known that P2 presents a more advanced chemical formulation than P1 producing a better finger definition. Both silver pastes have been provided by DuPont de Nemours Inc. Three of the four possible combinations have been implemented in the process line: the old one composed by P1 and S1 (named as P1@S1), the new one composed by P2 and the (P2@S2) and finally the combination of both, P2 and S1 (named as P2@S1). This third combination was considered because there existed a high S1 factory stock which had to be consumed if the power results were acceptable. The fourth combination, P1@S2 would not be implemented at the process line for the opposite reason, there was not an excess of P1 silver paste stock. The number of processed PV cells per front size metallographic design were: 1163, 1153 and 1932 units for P1@S1, P2@S1 and P2@S2, respectively. The printed finger per each serigraphy combination has been characterized both morphologically and electrically. The finger morphology was analyzed by field emission scanning electron microscopy (FESEM, FEI Helios Nano Lab 650) images and the variation in the contact resistance across the wafer has been measured with the CoreScan tool. The electrical characterization of the 4248 PV cells was carried out through the measurement of their I-V curve under standard conditions STC (irradiance of 1000 W/m^2, temperature equal to 25 °C, and incident spectrum AM1.5G), according to IEC 60904 (Millar et al., 2021; Kolster et al., 2020; Glass technical datasheet, 2022) in an AAA Class single-flash automatic solar cell tester (h.a.l.m. elektronik GmbH). The main parameters of the I-V curve under illumination conditions are short circuit current (I_{sc}), open-circuit voltage (V_{oc}), current intensity (I_{mp}), voltage at the maximum power point (V_{mp}), power at the maximum power point (P_{mp}) and fill factor (FF). The production results allowed to calculate the Lam-UP indicator and the serigraphy design impact.

The power increment due to the P2@S2 serigraphy design was confirmed by the controlled fabrication of 18 real size PV modules at the fully automated turnkey line supplied by Reis GmbH. The first stage of the production line is the clean out of the textured glass (3.2–4.0 nm thickness and 91.5 % transmittance) (EC 60904-3, 2019) and then, the front EVA foil is placed onto the inner part of the glass cover. Homogeneous diffusion screen printed monocrystalline silicon solar cells of 238.95 cm^2 area and pseudo-square shape, with a power range equal to [4.425–4.450) W were selected to build the solar device. They were connected along six strings (each string was formed by ten solar cell units), using a conductive copper string ribbon with an optimized section of 1.7 × 0.22 mm^2 and a sn-Bi-Ag alloy. To protect this assembly from the environmental agents, the rear EVA foil and the backsheet film were applied. The system was laminated in the lamination unit whose

process conditions were 140 °C, 300 s and 600 s for temperature, vacuum time and pressure time, respectively. After the system was allowed to cool down, the junction box was placed on the rear side of the solar module. The PV module I-V curves were measured in an AAA class solar module tester (Pasan S.A.) under standard conditions STC (irradiance of 1000 W/m^2, temperature equal to 25 °C and incident spectrum AM1.5G), according to IEC 60904-3 (Millar et al., 2021). The main parameters of the I-V curve are short circuit current (I_{sc}), open circuit voltage (V_{oc}), current intensity and voltage at the maximum power point (I_{mp} and V_{mp} respectively), power at the maximum power point (P_{mp}) and fill factor (FF). The final structural resistance is given by the anodized aluminum frame. Regarding the selected KIP, in this case CMR, was calculated and monitored for the whole production during a whole year. Finally, the produced PV module model evolution during the same year is also presented.

3. Results and discussions

3.1. Finger analysis

3.1.1. Morphological study

The main objective of this section is to obtain a morphological characterization of the front size metal serigraphy. Fig. 1 shows finger FESEM images per each of the three paste and screen-printing layout combinations considered: P1@S1, P2@S1 and P2@S2, Fig. 1 A-C, D-F and G-I, respectively. The finger plan views indicate notable definition differences between the three observed fingers. In the case of the P1@S1finger (Fig. 1 A), its edges along the whole metal line exhibit the lowest definition, which is an evidence of the high spread capacity of the P1 silver paste. When the P1 paste is replaced with the P2 paste but the screen-printing layout is the same than in the previous image, i.e. in the P2@S1configuration, a visible reduction of the lateral fringes can be noticed together with a slightly width reduction (Fig. 1D). The third analyzed front image belongs to the new paste (P2) together with the new screen-printing layout (S2), combination named as P2@S2 (Fig. 1G). This front view allows to determine that the P2@S2 combination leads to a well-defined finger footprint where the lateral fringes are significantly reduced, which leads to an increase in the photogeneration active area with respect to the P1@S1 and P2@S1 serigraphy combinations. The cross-section views also present useful information about the finger morphology per serigraphy design. The highest finger is obtained with the P2@S2 combination (Fig. 1H) followed by P2@S1 design (Fig. 1E) and finally the smallest front size serigraphy is defined by P1@S1structure (Fig. 1B). The cross-section images confirm the latter. The finger wide and height values per serigraphy combination are: 183.0 μm and 31.6 μm, 184.0 μm and 37.6 μm, 140.0 μm and 40.8 μm for the P1@S1 (Fig. 1 C), the P2@S1 (Fig. 1 F) and the P2@S2 (Fig. 1 I) combinations, respectively. These values indicate that the P2 front silver serigraphy paste allows to obtain higher finger footprints regardless of the mesh screen-printing layout.

3.1.2. Finger electrical characterization

The electrical properties of the finger for the various paste and screen-printing designs have been determined by the use of the CoreScan tool. This equipment biases the cell at the maximum power point and then measure voltage drops along the cell (Van der Heide, 1438). In this case, the method is automated to produce a map of the selected cells by paste and screen-printing serigraphy combination along with the evolution of the voltage drop across the cell as shown in Figs. 2 and 3, respectively. The colour evolution from a bluer map (in the case of P1@S1) to a more magenta map (P2@S2) are directly related with a better serigraphy electrical conduction (indicated by the lateral colour scale). In addition, higher contact resistance regions (marked with white circles) are presented in both maps. They are related with local problems, for instance cool spots during firing or contamination problems. In these cases, the defects are scratched of the emitter film (Fig. 2 A) and finger interruptions (Fig. 2 B and C).

In addition to obtaining the voltage drop map, the Corescan tool allows to perform a detailed voltage drop analysis across a transversal line with respect to the finger serigraphy. In this case, this line is located

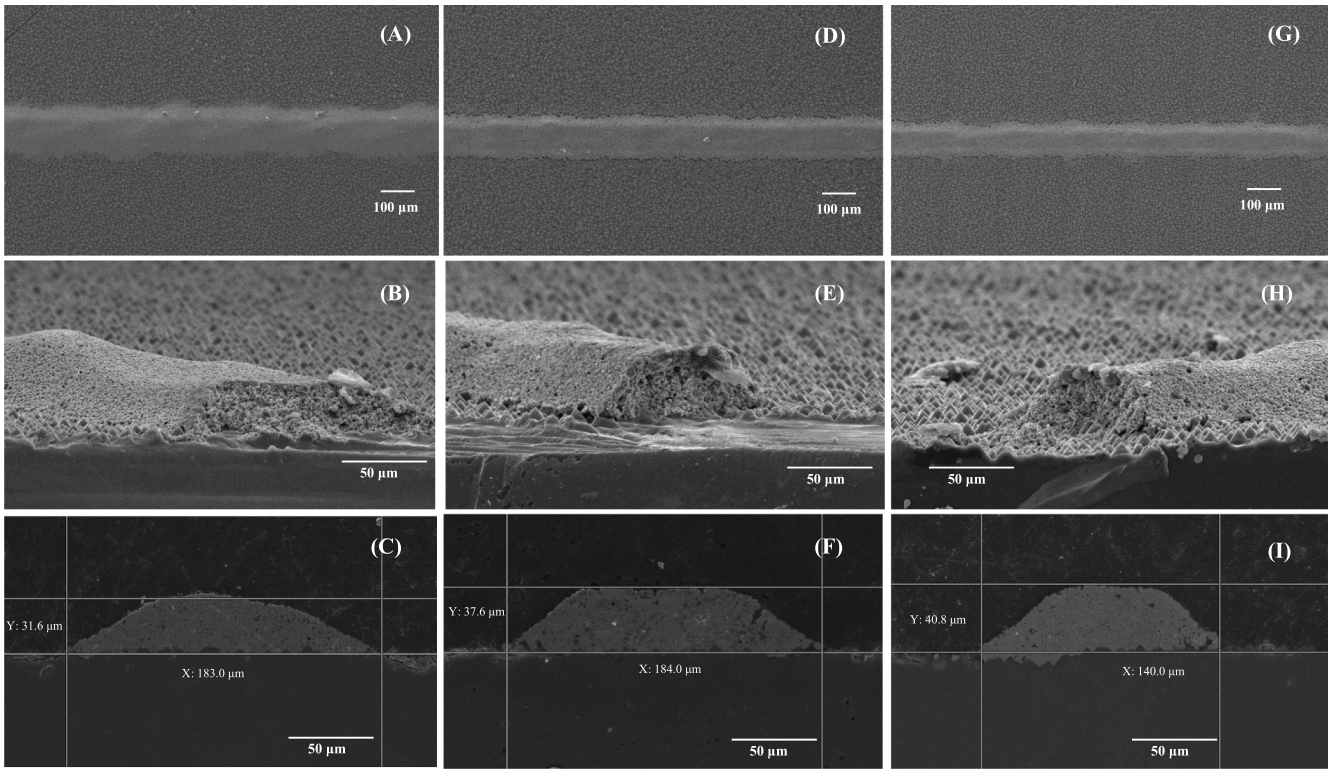

Fig. 1. P1@S1 (A, B, C); P1@S2 (D, E, F); P2@S2 (G, H, I).

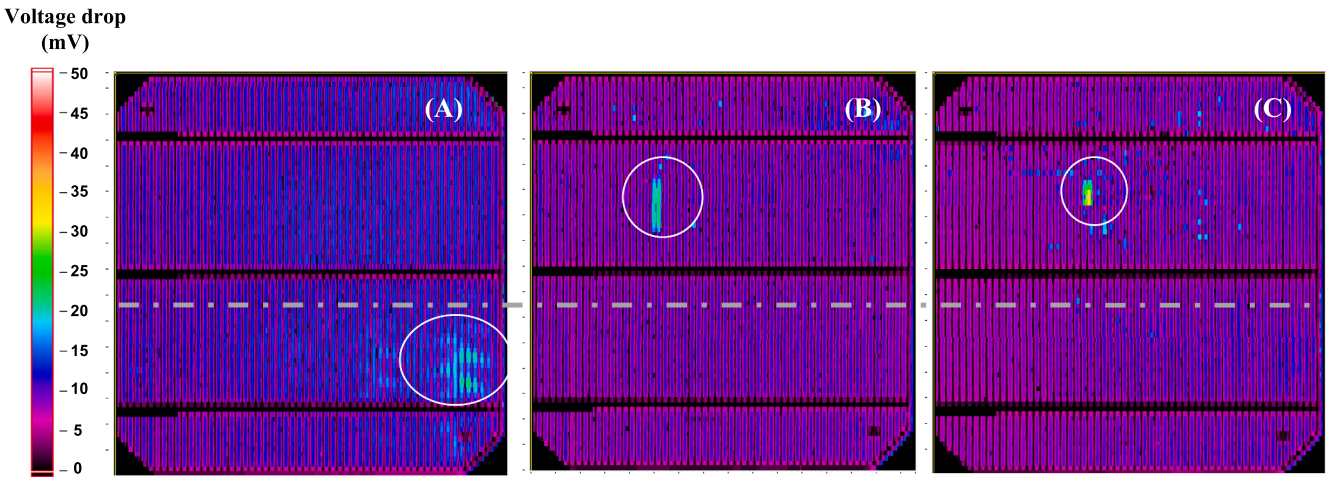

Fig. 2. Corescan map for three PV cells with the following serigraphy design: P1@S1 (A,); P1@S2 (B); P2@S2 (C).

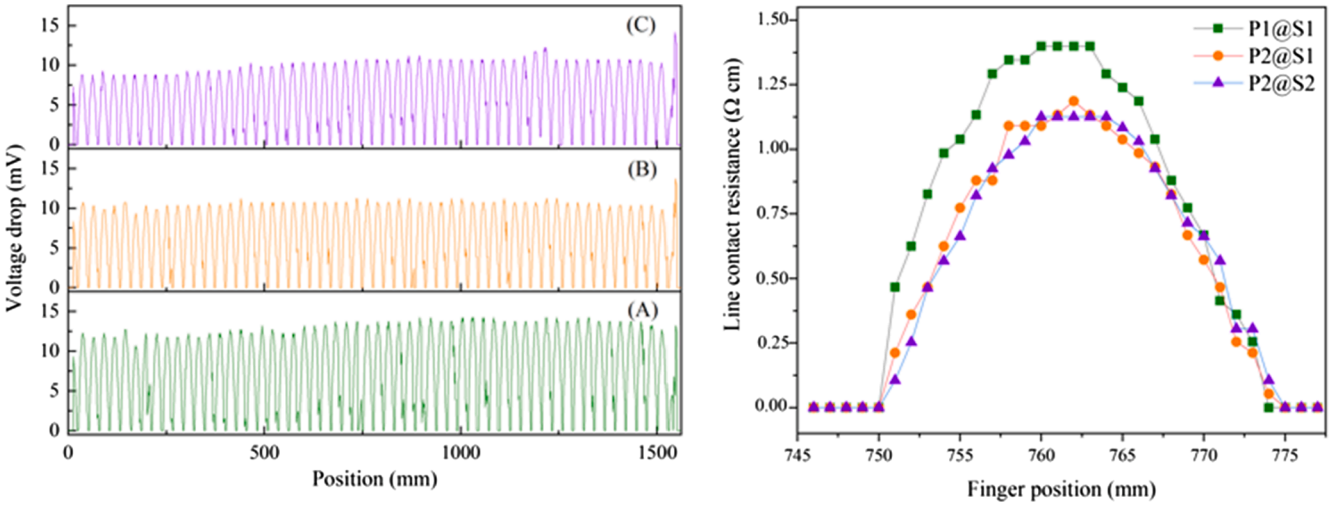

Fig. 3. (Left) Voltage drop evolution across a silicon solar cell transversal section for the following serigraphy design: P1@S1 (A); P1@S2 (B); P2@S2 (C). (Right) Line contact resistance of a finger for the three selected serigraphy combinations: P1@S1 (green,); P1@S2 (orange); P2@S2 (purple). (For interpretation of the references to colour in this figure legend, the reader is referred to the web version of this article.)

656 mm from the base of each PV cell and the line does not show any significant defect. The results are plotted in Fig. 3 left, where the voltage drop across the line has been represented per front size metal serigraphy combination: P1@S1, P2@S1 and P2@S2, Fig. 3 left A, B and C, respectively. The three graphs present 58 peaks related with each printed finger over the cell surface and the only difference between the graphs are the voltage drop values. The highest values are obtained for the P1@S1 front size metal configuration, where their maximum points lie between 12.5 mV and 14.1 mV. Obviously, these differences are not so evident for the other two configurations because they share the paste, and the only variation is the screen-printing serigraphy. As for P2@S1 and P2@S2, their maximum values are between 9.2 mV and 11.4 mV. Finally, these measurements allow to calculate the line contact resistance across a finger (R_{cl} expressed in Ω·cm). These calculations have been developed using Eq. (1), where V_{ce} is the voltage drop per point (mV), J_{sc} is the short current density (35.80 mA/cm^{-2}, 35.81 mA/cm^{-2} and 36.06 mA/cm^{-2} for P1@S1, P2@S1 and P2@S2, respectively) and d is the distance between two consecutive fingers (0.2637 cm). The results have been plotted in Fig. 3 right for the three selected configurations. Regarding the curve shapes, it is possible to observe how the P1@S1 printed finger (green line) is slightly wider than the other two fingers (P2@S1 and P2@S2, orange and purple lines respectively). This can be related with the silver paste composition which in the case of the P1 paste allows to a higher spreading over the silicon surface than the P2 paste, as SEM images prove. Concerning R_{cl} values, their maximus drop from 1.40 Ω·cm to 1.19 Ω·cm and 1.12 Ω·cm for P1@S1, P2@S1 and P2@S2, respectively.

$$R_{cl} = \frac{V_{ce}}{I_{sc} \bullet d} \tag{1}$$

3.2. Device electrical characterization: PV cells and modules

The main aim of this section is to analyze the effects of the front size serigraphy design on the cell and module production (3.2.1 section and 3.2.2 section, respectively). Both sections present the evolution of the main I-V curve parameters followed by the monitoring of the selected KPI.

3.2.1. Serigraphy design influence over silicon solar cell production

3.2.1.1. I-V parameter curve analysis. The way to evaluate the impact of the three front size serigraphy combinations on the silicon solar cell production is through the measurement of their I-V curves at standard

conditions. In this work three production batches have been defined, one per serigraphy combination with a similar number of solar devices: 1163 units, 1153 units and 1932 units for P1@S1, P2@S1 and P2@S2, respectively. With the aim to reduce the production uncertainty, the three batches have been processed consecutively using the same machine line. The only difference between the process of each batch is the silver paste (P1 or P2) and the screen printing (S1 and S2). The average value of the main I-V parameters is shown in Table 1 per cell power range and serigraphy configuration. The first principal difference between the three batches is related with the number of devices capable of the highest power range. The P1@S1 solar cells do not reach the higher power ranges above the [4.15–4.20) W range as opposed to the other two configurations which produce devices at the higher cell range, [4.30–4.35) and [4.25–4.30) W although with a significant difference in yield. In the case of [4.30–4.35) W, the numbers obtained are 1 and 23 for P2@S1 and P2@S2, respectively. A clearer picture of the latter can be obtained from the cell production histograms for the most significant power ranges of the three serigraphy configurations. This is represented in Fig. 4 and shows a general displacement towards higher power ranges and a more concentrated production in the case of the P2@S1 and P2@S2 configurations. A 79.09 % of the P1@S1 production is concentrated in two power ranges, between 4.05 and 4.15 W. For the second design, P2@S1, a 97.76 % of the production is concentrated in three power slots, between 4.10 and 4.25 W, with a 62.33 % falling inside the [4.15–4.20) W interval. Finally, the third metallography configuration, P2@S2 shifts the production upwards in power 96.31 % of the cells cluster between 4.15 and 4.30 W, the 59.15 % of the produced cells concentrating in the [4.20–4.25) range. Obviously, this behavior would imply a redistribution of the whole production depending on the serigraphy configuration.

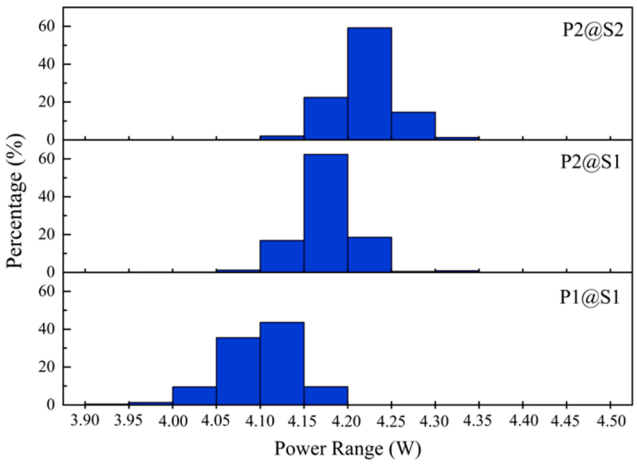

Fig. 4. Power histogram for each serigraphy combination. P1@S1 (bottom), P2@S1 (middle) and P2@S2 (top).

Back to the general analysis, Table 1 also shows the average values for the main I-V curve parameters, I_{sc}, V_{oc}, I_{mp}, V_{mp}, P_{mp} and FF per each metallic configuration. From a quality point of view and besides the power parameter, the main improvements are found at the current intensity parameters (I_{sc}, and I_{mp}). This is directly related with two serigraphy effects: the first one is the increase in active area due to the thinner fingers obtained with the P2@S1 and P2@S2 configurations, and the second one is the lower line contact resistance of the P2 paste. Regarding the voltage parameters, V_{oc} and V_{mp}, their variations are more related with the parameter dispersion inside of each power range

Table 1
I-V curve parameter average values of the fabricated silicon solar cells with the three serigraphy configurations: P1@S1, P2@S1 and P2@S2.

Configuration	Power Range (W)	Cell Number	I_{sc} (A)	V_{oc} (mV)	I_{mp} (A)	V_{mp} (mV)	P_{mp} (W)	FF (%)
P1@S1	4.30–4.35							
	4.25–4.30							
	4.20–4.25							
	4.15–4.20	5	8.47	618	7.99	522	4.16	79.71
	4.10–4.15	302	8.46	617	7.98	520	4.11	79.51
	4.05–4.10	597	8.42	615	7.95	518	4.07	79.43
	4.00–4.05	198	8.41	613	7.92	515	4.03	79.12
	3.95–4.00	28	8.45	614	7.94	511	3.98	78.13
	3.90–3.95	9	8.44	612	7.92	507	3.92	77.80
	3.85–3.90	1	8.42	619	7.84	504	3.87	75.84
	3.80–3.85	3	8.43	610	7.87	502	3.82	76.79
	3.75–3.80	1	8.41	610	7.82	501	3.75	76.35
	3.65–3.75	3	8.45	614	7.88	515	4.01	78.32
	3.55–3.65	3	8.44	615	7.94	518	4.08	79.22
	Total	1163						
P2@S1	4.30–4.35	1	8.58	618	8.15	519	4.31	79.76
	4.25–4.30	6	8.56	623	8.08	527	4.25	79.83
	4.20–4.25	207	8.57	621	8.09	524	4.21	79.67
	4.15–4.20	698	8.55	619	8.06	522	4.17	79.58
	4.10–4.15	185	8.52	617	8.03	519	4.13	79.38
	4.05–4.10	14	8.51	616	8.01	516	4.08	78.90
	4.00–4.05	2	8.60	617	8.06	511	4.04	77.62
	3.95–4.00	2	8.55	618	7.97	508	3.95	76.57
	3.55–3.95	18	8.68	617	7.82	519	4.02	75.86
	3.45–3.55	20	8.54	620	8.00	520	4.10	78.56
	Total	1153						
P2@S2	4.30–4.35	23	8.66	623	8.18	527	4.31	79.95
	4.25–4.30	253	8.66	622	8.18	524	4.26	79.12
	4.20–4.25	1025	8.64	619	8.16	522	4.22	78.84
	4.15–4.20	391	8.59	618	8.11	521	4.18	78.68
	4.10–4.15	36	8.53	617	8.05	519	4.13	78.43
	4.05–4.10	3	8.54	613	8.05	514	4.08	77.76
	4.00–4.05	1	8.47	615	7.96	515	4.03	77.36
	3.95–4.00	1	8.56	620	7.96	505	3.91	73.69
	3.55–3.95	190	8.62	619	8.10	521	4.19	78.45
	3.45–3.55	9	8.59	619	8.09	520	4.16	78.27
	Total	1932						

than with a process effect. The best way to have a more precise conclusion about the I-V curve evolution is to perform a detailed analysis of the best power range obtained for the three serigraphy combinations. With this aim, more silicon solar cells were processed until a substantial cell number in the [4.00–4.50) W power range for the P1@S1 and P2@S1 serigraphy configurations was obtained. Nominally, 275 units, 207 units and 1025 units were produced for P1@S1, P2@S1 and P2@S2, respectively. Their main I-V parameters have been represented as a boxplot and are shown in Fig. 5. The Boxplot diagrams represent 50 % of the observations using vertical boxes while the rest of the measurements are drawn as whiskers, with 25 % of the distribution at the top of the box and the remaining 25 % at its bottom. Even if the analysis is referred to the same power range, the I_{sc} current parameter, shows an upward trend with the evaluated designs. increase. The average value for this parameter is 8.51 A, 8.58 A and 8.64 A for P1@S1, P2@S1 and P2@S2, respectively (the outliers in the P2@S2 boxplot are related with the higher number of cells accounted for). The voltage parameter boxplot, V_{oc}, exhibits a slight decrease with values equal to 622 mV, 622 mV and 620 mV for P1@S1, P2@S1 and P2@S2, respectively. The lower P2@S2 value is related with process itself (different silicon wafer resistivity, process effects, etc.). Regarding the power boxplot graph, P_{mp}, P1@S1 and P2@S1 show average values equal to 4.219 W and 4.216 W which are nearer to the lower part of the [4.20–4.25) W interval, while P2@S2 has an average value of 4.224 W, at the center of the interval. Finally, the fill factor parameter, FF, does not show significant differences between the serigraphy configurations because the differences are compensated between the considered current, voltage and power parameters.

3.2.1.2. Solar cell key performance indicators. Solar cell KPI allow quantitative monitoring of the most significant production parameters. In this work, the selected KPI is the Laminated Unit Power (Lam-UP) which represents the average power produced by cells that can be laminated (power higher than 3.650 W and without any aesthetic defect). As cell production is sorted in power ranges, the power value assigned to each group is the lower bound of the interval. For instance, a hypothetical amount of 250 units in the power range of [4.20–4.25) W would be declared as 250 units of 4.20 W. Eq. (1) presents the calculation of the Lam-UP parameter where P_{min} is the lower bound of the range, $n_{cell\ range}$ is the produced cell in each considered cell range and n_t is the total considered cell number.

$$Lam-UP = \frac{\sum\left(P_{\text{minpercellrange}} \bullet n_{cellrange}\right)}{n_{total}} \quad (2)$$

Lam-UP is continuously calculated and it is linked to the different silicon suppliers as well as to the used production machines. In Fig. 6, the Lam-UP analysis is presented over the month in which the serigraphy design changed from P1@S1 to P2@S2 and in two situations: taking into account only the most abundant silicon supplier (red line) or considering all the processed silicon suppliers (black line). The daily production is approximately 65,135 units comprising the various suppliers.

This graph shows two well differentiated regions where the Lam-UP value experiments a substantial increment -marked by a discontinuous vertical line- which coincide with the serigraphy design change: from P1@S1with an average value of 4.08 W to P2@S2 with an average value of 4.20 W for the whole processed suppliers. With regards to the differences between the two plots at the same point in time (production day), they are directly related with the number of cells processed for the selected silicon supplier. It is normal that the process of final silicon wafer reception grouped units with some small deviations (for example in wafer resistivity or carried lifetime) which generates the observed deviations from the general black line.

The Lam-UP parameter analysis along a year shows the impact of the serigraphy design change over the silicon solar cell production, taking in

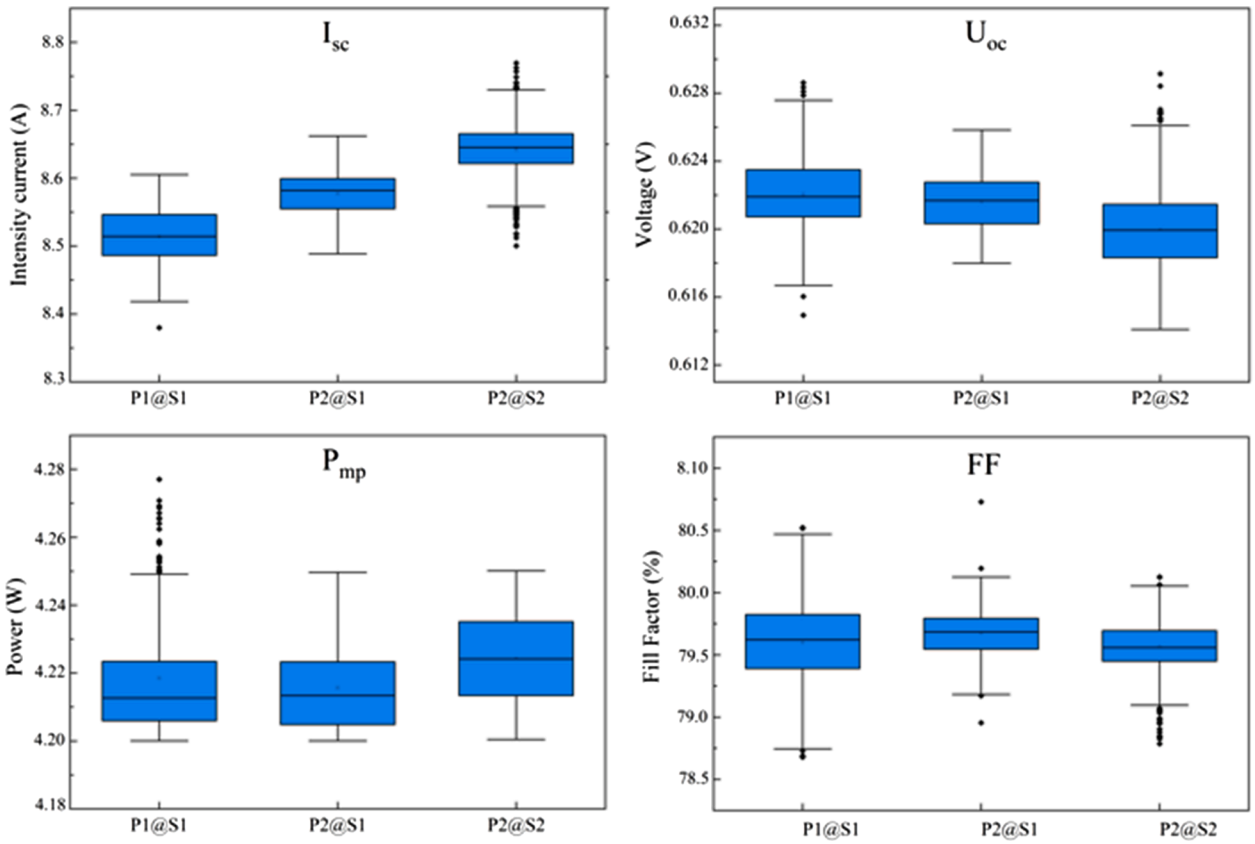

Fig. 5. Boxplot of the main I-V parameters for the three serigraphy combinations: P1@S1, P2@S1 and P2@S2.

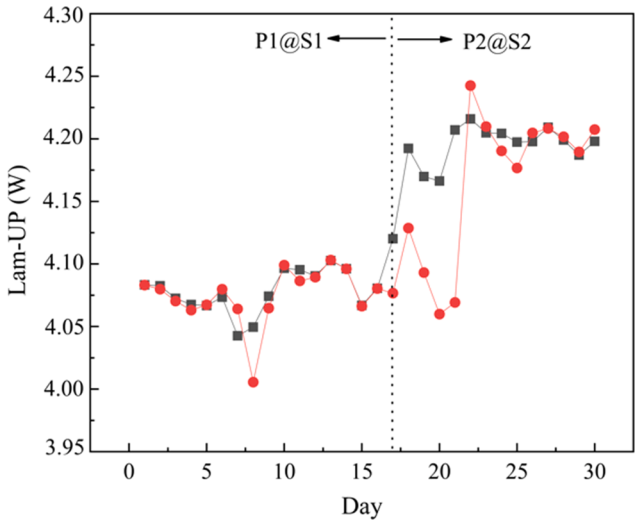

Fig. 6. Laminated united power evolution along a month for the major silicon wafer supplier (red line) and for all the silicon wafer suppliers (black line). (For interpretation of the references to colour in this figure legend, the reader is referred to the web version of this article.)

main that in such type of factories the implementation of new developments is a continuous task which can cause slight oscillations. Fig. 7 shows the evolution of Lam-UP parameter along the year for the two principal silicon wafer suppliers (red and blue lines) and for the whole processed silicon wafer suppliers (black line). This graph presents a general ascendant trend for the three lines with a most severe slope located along the month of June when the serigraphy design was changed from P1@S1 to P2@S2. Before this moment Lam-UP values vary between 3.95 W and 4.07 W with singular deviations related with the number of processed batches per silicon wafer supplier as has been commented in Fig. 6. The slope increment can be observed during the months of middle of May and July which Lam-UP global values are equal to 4.13 W and 4.15 W. During these two months, the two serigraphy designs, P1@S1 and P2@S2, were used in metallization production stage until P1 paste and S1 screen printing stocks were used up. A small quantity of wafers was processed with P1@S2 combination due to the high S2 stock. The rest of the year just P2@S2 combination is the unique

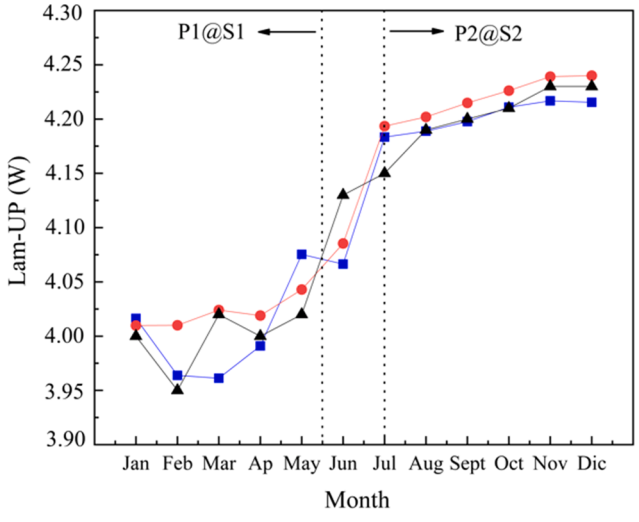

Fig. 7. Laminated united power evolution along a year for the two majority silicon wafer suppliers (red and blue lines) and for all the processed silicon wafer suppliers (black line). (For interpretation of the references to colour in this figure legend, the reader is referred to the web version of this article.)

implemented in the production line and the Lam-UP global value goes from 4.19 W to 4.23 W. The former increment is related with other small improvements at wet line or diffusion stage which are out of the scope of this work.

3.2.2. Serigraphy design influence over real size PV module production

3.2.2.1. I-V curve parameter analysis. The PV module performance is influenced by the improvement carried out at cell level. With the aim to determine the achievable power, eighteen real size PV modules were fabricated in an automatic-industrial line using PV silicon solar cells with the P2@S2 serigraphy combination and two different cell power ranges. Overall, 14 modules were fabricated from cells in the [4.200–4.250) range and 4 modules with cells from [4.250–4.300) W range. The main I-V curve average parameters are shown in Table 2 grouped by cell power range along with the cell to module ratio (CMR). CMR is the relative difference between the measured P_{mp} ($(P_{mp})_m$) and the P_{mp} of a PV module processed with the same PV cell power range without any performance loss ($(P_{mp})_{ideal}$) (Eq. (2)).

$$CMR = \frac{(P_{mp})_m - (P_{mp})_{ideal}}{(P_{mp})_{ideal}} \times 100. \quad (3)$$

Table 2 shows the PV module I-V curve parameter average values for the two cell power ranges. From a general point of view, this table indicates that the main parameters measured are very similar. The only parameter which presents a notable difference is I_{mp} for which an increase of 40 mA was measured. This current improvement is the responsible of the difference of the module P_{mp} between the two cell ranges selected. Regarding the PV module classification, the solar devices are sorted in discrete intervals of 5.0 W, so both cell ranges lead to 235 W although with a difference in the position inside the power interval where the higher cell power range leads to PV modules in the center of the interval.

3.2.2.2. PV module key performance indicators. In this subsection, the influence of the P2@S2 serigraphy implementation over the CMR parameter is studied. This PV module KPI is analyzed over a whole year.

In PV module factories, the PV cells are received in packages of 100 units where the devices have been previously sorted by its P_{mp} value in discrete power ranges, for example [4.200–4.250) and [4.250–4.300) W with average values of 4.225 W and 4.275 W, respectively. In fact, this average value is used to refer the cell power range and to distinguish the evolution of KPI by products. CMR monitoring can be considered as a KPI which provides valuable information about the line performance, mainly when it is associated to cell power range. Fig. 8 presents the obtained CMR value in each year quarter (Q1, Q2, Q3 and Q4 which are represented in orange, green, purple, and yellow colors) for all power ranges. If attention is paid to the CMR evolution for each processed cell power range, it is possible to observe that not all the cell types have been assembled along the year. This fact affects to the most extreme cell ranges: 3.925 W and 3.975 W which have not been processed in Q4 in addition to 4.225 W, 4.275 W and 4.325 W which have not been processed in Q1. This is directly related with the power increase developed at the cell level, which was implemented over Q3. The P2@S2 serigraphy combination leads to a redistribution of the fabricated cell power ranges upwards to higher performance devices (shown in Fig. 4). Moreover, Fig. 8 also presents a general decrease of the CMR value regardless of the assembled cell power range. This is related with the cell technology, which implies that the most common produced cell ranges tend to be in the higher end of its narrow power interval, while the most extreme processed cell power ranges tend to be displaced from the center of the interval. Finally, it is possible to observe that the CMR value grows with the cell power range. This fact is related with the serial resistance of the copper tab ribbons as regardless of the PV module power, the conductive transversal section is always the same, leading to

Table 2
I-V curve parameter values of the fabricated PV modules with the P2@S2 serigraphy configuration.

Cell power range (W)	Device number	I_{sc} (A)	V_{oc} (V)	I_{mp} (A)	V_{mp} (V)	P_{mp} (W)	FF (%)	CMR (%)
4.225	14	8.48	36.84	7.89	30.01	236.84	75.79	6.0
4.275	4	8.49	36.85	7.93	29.98	237.65	75.95	6.8

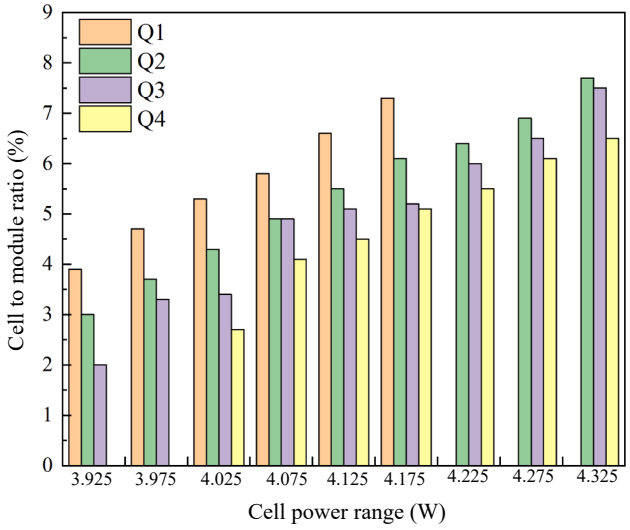

Fig. 8. CMR value for all assembled power ranges over a year: the four quarters, Q1, Q2, Q3 and Q4 are depicted in orange, green, purple and yellow, respectively. (For interpretation of the references to colour in this figure legend, the reader is referred to the web version of this article.)

high serial resistance for the higher the PV module power.

Regarding the model distribution of the PV module produced along the year, five PV module models were monitored. In particular, 220 W, 225 W, 230 W, 235 W and 240 W. which correspond to the classification of the production with the power ranges of [220–225) W, [225–230) W, [230–235) W, [235–240) W and [240–245) W, respectively. Their production percentage has been depicted per year quarter and the obtained distribution is presented in Fig. 9. This bar graph illustrates that during the first half of the year, four out of the five PV module models studied

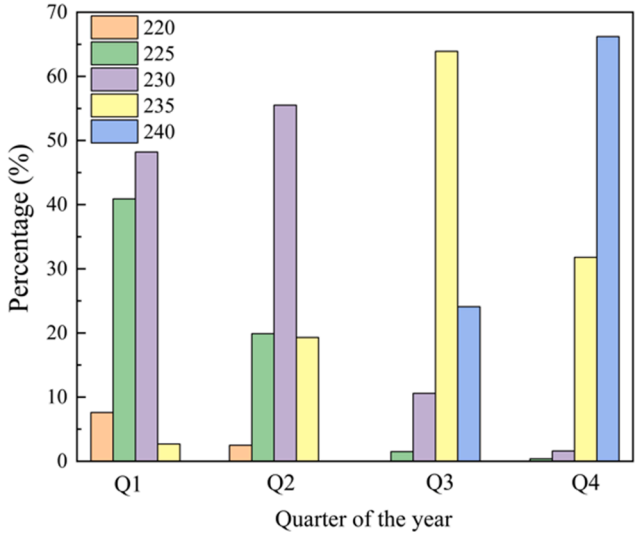

Fig. 9. Percentage distribution per PV module model over a year. The monitored PV module models are: 220 W, 225 W, 230 W, 235 W and 240 W, which have been indicated by the following colors and in the same order: orange, green, purple, yellow and blue, respectively.

were fabricated, the most produced product being the 230 W module with percentages of 48.2 % and 55.5 % for Q1 and Q2, respectively. It is also possible to observe a slight improvement in the 235 PV module model during the second year-quarter which raises from 2.7 % to 19.3 % in detriment of the 225 PV module model. But without a doubt, the great change in the distribution of produced modules occurs in the second half of the year (Q3). During the third year-quarter, 98.5 % of the production is concentrated in the three higher PV module models: 230 W, 235 W and 240 W with percentages of 10.6 %, 63.9 % and 24.1 %, respectively. This is directly related with the introduction of the P2@S2 serigraphy combination at cell level. Q4 shows better results due, on the one hand, to the depletion of the P1 and S1 stocks, and on the other hand, to the consolidation of the P2@S2 technology. These two factors allow to finish the year with a 99.6 % of the production concentrated in the same three best models 230 W, 235 W and 240 W with a distribution equal to 1.6 %, 31.8 % and 66.2 %.

4. Conclusions

A successful monitoring of the implemented in-line serigraphy changes have been developed by the selected key performance indicators with the aim to carried out a quantitative valuation of the power improvement in commercial PV cells and modules. The three most viable combinations have been tested in real size front size serigraphy cells production lines: P1@S1, P2@S1 and P2@S2 which correspond to old and new front size silver pastes (P1 and P2) and screen-printing layouts (S1 and S2), respectively.

Previous to the power measurement, each front size serigraphy design has been characterized and SEM images show an actual improvement of the printed finger when the P1@S1 serigraphy design is replaced by the P2@S2 combination. Finger width and height changes from 183.9 μm and 31.6 μm to 140 μm and 40.8 μm for P1@S1 and P2@S2, respectively. The finger contact resistance measurement also indicated an improvement with drops from 1.40 Ω·cm to 1.12 Ω·cm for P1@S1 and P2@S2, respectively. With respect to the P1@S2 design, their finger dimensions and contact resistance values are among those indicated for each parameter.

The intensity–voltage curve measurement of the cells produced with each serigraphy design indicate a correlation between their parameters and their finger properties. Since the P2@S2 configuration implies an enhancement of the silicon active region, the improved parameter is the current intensity which implies a modification of the produced cell histogram. In the case of the most produced cell power range, it is displaced from [4.10–4.15) W and [4.15–4.20) W to [4.20–4.25) W for the P1@S1, P2@S1 and P2@S2 configurations, respectively. Moreover, the P2@S2 combination was able to produce 23 units of the [4.30–4.35) W power range. This enhancement in cell power was successfully monitored by the selected key performance indicator: laminated unit power parameter, which increased from 3.95 W to 4.15 W when the P1@S1 design was replaced by P2@S2 combination.

Concerning the photovoltaic module results, the controlled fabrication of 235 W model with the first [4.20–4.25) W and [4.25–4.30) W cell batches of the P2@S2 design has been demonstrated. PV module model production results indicate an evolution related with serigraphy modification, 230 W being the most produced model during the first three-month period (48.2 %) while the 240 W model was the most produced module during the fourth three-month period (66.2 %). Regarding the key performance indicator at module level, the selected one has been the cell to module ratio per module model. In general, this indicator

presented higher values for better module models and the optimization of the cell process parameters led a decrease of the KPI for the same module model. In this way, the cell to module ratio for modules produced with [4.30–4.35) W cells in the first and fourth four-month period, decreased from 7.7 W to 6.5 W.

Declaration of Competing Interest

The authors declare that they have no known competing financial interests or personal relationships that could have appeared to influence the work reported in this paper.

Acknowledgements

The authors are thankful to Erasmus+ Programme, SafeEngine project, contract no 2020-1-RO01-KA203-080085, Spanish Ministerio de Ciencia e Innovación through project PID2020-117832RB-100, UMA 18-FEDERJA-041 for their support and to Isofoton and J. Alcaide and J. Rando from 4TENERGY S.COOP:AND, for their collaboration.

References

Bhadani, K., Asbjörnsson, G., Hulthén, E., Evertsson, M., 2020. Development and implementation of key performance indicators for aggregate production using dynamic simulation. Miner. Eng. 145.

Caballero, L.J., 2010. Contact definition in industrial silicon solar cells. https://www.intechopen.com/books/solar-energy/contact-definition-in-industrial-silicon-solar-cells. Published: February 1st 2010, doi: 10.5772/8075.

Chauvy, R., Meunier, N., Thomas, D., De Weireld, G., 2019. Selecting emerging CO2 utilization products for short-to mid-term deployment. Appl. Energy 236, 662–680.

Current price and price trend of gold and silver. Available "https://www.goldpreis.de/silberpreis/" [accessed: 11- January-2022].

EC 60904-3:2019. Photovoltaic devices – Part 3: Measurement principles for terrestrial photovoltaic (PV) solar devices with reference spectral irradiance data.

Ferrer, B.R., Muhammad, U., Mohammed, W.M., Matínez Lastra, J.L., 2018. Implementing and visualizing ISO 22400 Key Performance Indicators for Monitoring Discrete Manufacturing Systems. Machines 6, 39. https://doi.org/10.3390/machines6030039.

Gallo, M., Costabile, C., Sorrentino, M., Polverino, P., Pianese, C., 2020. Development and application of a comprehensive modern-based methodology for fault mitigation of fuel cell powered systems. Appl Energy 279.

Glass technical datasheet. Available https://www.guardianglass.com/ru/en/our-glass/solar-control-glass [accessed: 26- June-2022].

Glunz, S.W., 2007. High-Efficiency Crystalline Silicon Solar Cells. Hindawi Publishing Corporation. Advances in OptoElectronics, 2007, Article ID 97370, 15 pages, doi: 10.1155/2007/79370.

Glunz, S.W., 2007. High-Efficiency Crystalline Silicon Solar Cells. Hindawi Publishing Corporation. Advances in OptoElectronics, 2007, Article ID 97370, 15 pages, doi: 10.1155/2007/79370.

Hörteis, M., Glunz, S.W., 2008. Fine line printed silicon solar cells exceeding 20% efficiency. Prog. Photovolt.: Res. Appl. 16, 555–560.

https://www.bp.com/content/dam/bp/business-sites/en/global/corporate/pdfs/energy-economics/energy-outlook/bp-energy-outlook-2020.pdf [accessed: 11- January-2022].

https://www.bp.com/content/dam/bp/business-sites/en/global/corporate/pdfs/energy-economics/statistical-review/bp-stats-review-2021-full-report.pdf [accessed: 11- January-2022].

https://www.miteco.gob.es/es/cambio-climatico/temas/el-proceso-internacional-de-lucha-contra-el-cambio-climatico/naciones-unidas/elmentos-acuerdo-paris.aspx [accessed: 11- January-2022].

https://ukcop26.org/cop26-goals/ [accessed: 11- January-2022].

https://ec.europa.eu/clima/policies/strategies/2050_en [accessed: 11- January-2022].

https://itrpv.vdma.org/documents/27094228/29066965/2021%30ITRPV/08ccda3a-585e-6a58-6afa-6c20e436cf41 [accessed: 11- January-2022].

Hu, M., Zhao, B., Ao, X., Ren, X., Cao, Y., Wang, Q., Su, Y., 2020. Perfromance assessment of a trifunctional system integrating solar PV, solar thermal and radiative sky cooling. Appl Energy 260.

Jäger-Waldau, A., 2022. ISBN 978-92-76-12608-9. ISSN 1831-9424, doi:10.2760/326629. Available at https://ec.europa.eu/jrc/sites/jrcsh/files/kjna29938enn_1.pdf [accessed: 11- January-2022].

Kolster, T., Krebs, R., Niessen, S., Duckheim, M., 2020. The contribution of distributed flexibility potentials to corrective transmission system operation for strongly renewable energy system. Appl. Energy 279 (1).

Kourkoumpas, S., Benekos, G., Nikolopoulos, N., Karellas, S., Grammelis, P., Kakaras, E., 2018. A review of key environmental and energy performance indicators for the case of renewable energy systems when integrated with storage solutions. Appl. Energy 23, 380–398.

Kourkoumpas, D.S., Benekos, G., Nikolopoulos, N., Karellas, S., Grammelis, P., Kakaras, E., 2018. A review of key environmental and energy performance indicators for the case of renewable energy systems when integrated with storage solutions. Appl. Energy 231, 380–439.

Li, J., Jurasz, J., Li, H., Tao, W.Q., Duan, Y., Yan, J., 2020. A new indicator for a fair comparison on the energy performance of data centers. Appl. Energy 276.

Kriebel, D., 2001. Lowell center for sustainable production. Approaches to sustainable development: the public university in the regional economy, 295.

Matino, I., Colla, V., Baragiola, S., 2017. Quantification of energy and environmental impacts in uncommon electric steelmaking scenarios to improve process sustainability. Appl. Energy 207, 543–552.

May, G., Barletta, I., Stahl, B., Taisch, M., 2015. Energy management in production: A novel method to develop key performance indicators for improving energy efficiency. Appl. Energy 149, 46–61.

Millar, M.A., Yu, Z., Burnside, M., Jones, G., Elrick, B., 2021. Identification of key performance indicators and complimentary load profiles for 5th generation district energy networks. Appl. Energy 291.

Navas-Anguita, Z., Garcia-Gusano, D., Dufour, J., Iribarren, D., 2020. Prospective techno-economic and environmental assessment of a national hydrogen production mix for road transport. Appl. Energy 259.

Papetti, A., Menghi, R., Di Domizio, G., Germani, M., Marconi, M., 2019. Resources value mapping: A method to assess the resource efficiency of manufacturing systems. Appl. Energy 249, 326–342.

Salahi, N., Jafari, M.A., 2016. Energy-Performance as a driver for optimal production planning. Appl. Energy 174, 88–100.

JRC Science for Policy Report. PV Status Report 2019. Available at https://publications.jrc.ec.europa.eu/repository/handle/JRC118058 [accessed: 11- January-2022].

United Nations, 2015. Transforming our world: The 2030 agenda for sustainable development. Resolution adopted by the General Assembly; 2015. Available at https://www.un.org/en/development/desa/population/migration/generalassembly/docs/globalcompact/A_RES_70_1_E.pdf. [accessed: 11- January-2022].

United Nations, 2015. Transforming our world: The 2030 agenda for sustainable development. Resolution adopted by the General Assembly; 2015. Available at https://www.un.org/en/development/desa/population/migration/generalassembly/docs/globalcompact/A_RES_70_1_E.pdf. [accessed: 11- January-2022].

Van der Heide, A.S.H., 2000. Mapping of contact resistance and locating shunts on solar cells using Resistance Analysis by Mapping of Potential (RAMP) techniques. In: 16th European Photovoltaic Solar Energy Conference. Glasglow (United Kingdom) p. 1438, 2000. Available: https://www.osti.gov/etdeweb/biblio/20098255 [accessed: 26-June-2022].